

ScienceDirect

MANUFACTURING

Procedia Manufacturing 00 (2020) 000-000

www.elsevier.com/locate/procedia

49th SME North American Manufacturing Research Conference, NAMRC 49, Ohio, USA

Assessing laser powder bed fusion system geometric errors through artifactbased methods

J. Berez^{a*}, M. Praniewicz^a, C. Saldana^a

^aGeorgia Institute of Technology, George W. Woodruff School of Mechanical Engineering, 801 Ferst Dr., Atlanta, GA 30332, USA

* Corresponding author. Tel.: +1-301-943-7525. E-mail address: j.berez@gatech.edu

Abstract

Additive manufacturing (AM) machines have developed more rapidly than standardized frameworks needed for the qualification of their geometric capabilities. While some manufacturer-specific methods exist to test capabilities and perform some calibration tasks, standardization efforts have only recently been undertaken in the form of ISO/ASTM 52902. In this study, the recommended methodology prescribed by the standard was implemented by building geometric artifacts with a laser powder bed fusion (LPBF) system and performing dimensional inspection with a coordinate measurement machine (CMM), amongst other methods. Typical dimensional capabilities of the LPBF system are identified and commentary is made on applying metrology methods, detecting geometric error, and diagnosing base causes in the LPBF system. In doing so, favored metrology practices and measurement analysis methods auxiliary to the standard are proposed. Artifact measurements were used to characterize beam positioning error and beam offset error. Methods for decoupling the effects of error sources are proposed. Difficulties in the inspection of AM components are identified, and the effects of various CMM measurement strategies are evaluated. Insights on the application of the new standard are presented, along with commentary as to its fitness for the LPBF process.

© 2019 The Authors, Published by Elsevier B.V.

Peer review under the responsibility of the scientific committee of NAMRI/SME

Keywords: ISO/ASTM 52902, additive manufacturing, geometric artifact, geometric benchmark, machine qualification, metrology

1. Introduction

maturation of metal additive manufacturing technologies in recent years has led to their adoption not just in the field of rapid prototyping but also in production environments. This development has necessitated that a suite of qualification techniques be aimed at AM in order to ensure component quality and define limits of acceptable process characteristics. This particularly applies to metal-AM components, as their applications are often more demanding and come with additional qualification requirements [1]. Efforts in this area are wide-ranging and can be said to largely focus on qualifying an AM process, i.e., understanding outcomes of the physics that contribute to the quality of a manufactured component. Examples of these qualification efforts include porosity detection, in-situ monitoring, microstructural examination, and mechanical property determination [2]. Notably, many of these methods do not focus on qualifying the AM machine itself, leaving a considerable gap in the knowledge of factors that contribute to the outcome of an AM process and machine pairing, i.e. an AM system [3].

Once such gap in AM system qualification research is characterization of the geometric capabilities, errors, and error sources of AM machines, i.e. machine geometric qualification [4]. Purchasers of AM systems require knowledge of system construction quality and capability that the machine manufacturer can readily communicate. Machine end-users must also be able to monitor system performance and take corrective action if needed. Further, in many production environments, manufacturing system geometric performance must be quantified in such a way that links to verifiable and mutually understood qualification techniques [3], [4].

Two generalized approaches can be taken to address these needs – direct machine evaluation, e.g. evaluation of build platform or laser beam positioning system errors, or evaluation of the AM system, e.g. evaluation of a component produced by

the system that captures aspects of both the machine and process [3], [4]. This concept of evaluating an AM system via a manufactured artifact has garnered significant research and standardization efforts of late. This paper will examine the application of ISO/ASTM 52902, one such standardization effort recently put forth [5].

2. Background

Machine qualification realized through either direct or system-level evaluation is a familiar concept in the manufacturing field. Machine tools used in subtractive processes are bolstered by considerable infrastructure when it comes to the tasks of assessing geometric capabilities and extracting information for machine calibration. Direct measurement of the errors in a machine tool has long been an area of study and industrial focus [6], [7]. Additionally, standards have been evolving since as early as since as early as 1969 which describe the procedures for manufacture and inspection of test articles that allow for diagnosis of machine geometric characteristics [8]–[10].

The need for similar practices in relation to AM machines has grown evident [4], [11], [12]. An advantage of using manufactured artifacts in this context is that all constitutive error sources, whether based in the process or machine, are captured [3], [13]. In powder-bed metal AM systems this approach can include effects due to powder size, heat source and scan settings, and resultant meltpool geometry – aspects direct measurement of the machine would not capture [3]. However, there are downsides to the artifact measurement approach, in that the complex combination of error sources may obfuscate underlying causes. This may be a necessary tradeoff, as direct control of the sub-systems in commercial AM machines is often not possible nor easily measured with readily available equipment [3], [4]. In comparison, artifacts are generally suited to measurement with common industrial tools.

Some of the earliest references to a geometric artifact for AM processes come from Kruth in 1991 [14]. Artifacts have been critical to representing the geometric capabilities of an AM system thereby allowing system comparisons [15], [16]. A great many geometric artifacts, also frequently known as benchmark test artifacts, have been conceived and built with many different methodologies and primary purposes. Several authors have conducted extensive reviews on the topic [4], [11], [12], [17]. In general, prior efforts have attempted to design artifacts that subscribed to design rules put forth by Richter and Jacobs while also occasionally advocating for other good practices [18]. Artifacts generally include a variety of feature types intended to assess geometric limits of the AM system at hand (e.g., maximum overhang angle, minimum feature size), repeatability (e.g. spatial, build-to-build, or machine-tomachine repeatability), or achievable geometric characteristics (e.g. flatness, cylindricity, position, etc.). Framing machine geometric performance in the context of a rigorous geometric dimensioning and tolerancing (GD&T) definition has been emphasized [13], [19]. Recent work has advocated for a design approach, which acknowledges for metrology measurement tools and strategies have a significant impact on the outcome of an article inspection [20].

It is worth noting that many of these efforts are somewhat focused on benchmarking goals, i.e., restricted to comparing capabilities or simply quantifying achievable geometry. That said, several works have strived to utilize artifacts to also aid in machine qualification. In this area Kruth et al. has suggested artifact designs that promote iterative improvements to the process [21]. Byun and Lee noted that artifacts should be oriented in machine coordinate directions in order to allow for more direct assessment of machine and process errors [22]. Scaravetti et al. emphasized the importance an artifact design whose measurands can be used to qualify an AM machine. Mitchel et al. took a similar approach in the context of metal AM [23]. Brøtan and Tang et al. each have made efforts to quantitatively assess geometric errors inherent to LPBF machines through artifact measurement as well [24], [25]. One prevalent artifact design, which has been duplicated in various works, was developed Moylan et al., and is commonly known as the 'NIST artifact' [26]. This design was primarily intended for metal AM systems and was developed to test the limits of achievable feature size as well as evaluate system geometric capabilities with an insight as to the base sources of error in the machine and process.

In 2019, the F42 work committee of ASTM published the first standard that encompasses AM geometric artifact design and use. The standard was a joint venture with ISO, and is titled "ISO/ASTM 52902-19 - Additive manufacturing - Test artifacts - Geometric capability assessment of additive manufacturing systems" [5]. In the area of article design, the overall hierarchy of the standard is designed to allow for configurability and flexibility. There is no single artifact prescribed, rather a set of individual artifact geometries are defined. While comments are made as to how a combination of artifacts can be used in a single build to form an overall test piece only an example is provided, and no single best practice defined. Given that AM machines vary in build volume, capability, and construction, this approach appears to be favored by the standard authors as it allows for a measure of uniformity while meeting many user's needs. Additionally, this strategy reduces build time and feedstock material consumption. Multiple appropriate measurement methods are provided for each geometric artifact along with notes on their implementation. However, it is fair to say that measurement methodology is minimally prescribed, and choice of method is generally left up to the user.

At this moment, the authors are not aware of any publications that have discussed the direct implementation of ISO/ASTM 52902 on an AM system. In this work, the standard is used with a LPBF system to study its application and overall fitness as well as derive AM system geometric capabilities, error trends, and error sources. It is shown that implementation is non-trivial and that rigorous analysis methods, such as those developed by the authors, are critical when relating particular artifact measurands to a meaningful AM machine diagnosis. Detailed and deliberate methods of identifying error and decoupling error sources are proposed. The effects of CMM measurement strategies on several measurands are studied, and particular problems in AM metrology are highlighted. It is also shown that the choice of measurement strategy can significantly bias measurement results. Finally, a critique of the

standard is provided, and suggestions made as to its future application.

3. Methodology

3.1. Test piece design

As earlier described, the standard does not provide a single configuration or combination of artifacts that should be utilized in the manufacture of a single overall test piece. A test piece was designed for this study according to the broad guidelines of the standard which are be summarized below.

- Build plate coverage should be 80% or greater
- Small artifacts that test machine capabilities may fail; they should be arranged to avoid affecting other artifacts
- Long, semi-continuous artifacts that span the build area should be used to detect non-linear effects
- Provided artifact designs should not be scaled, although they be arrayed
- Supports should be avoided, and the test piece should be designed to not require post-processing prior to inspection

All seven classes of artifacts were included in the test piece: linear artifacts, circular artifacts, resolution pins, resolution holes, resolution ribs, resolution slots, and surface texture artifacts. The linear, circular, and surface texture artifacts designs are provided at several size scales for the user to select from. Each of the resolution type artifacts has several possible configurations defined for the user to select from – coarse, medium, or fine – allowing for a configuration to be chosen that spans the AM system's capabilities.

The designed test piece can be seen in Fig. 1, and close-up views of each artifact can be found as insets in later figures. Artifacts are shown on the build plate, as they were measured. Note the coordinate system which is defined as originating on the build area center with the +Z direction matching the build direction. Linear artifacts (LA) were arranged to cover most of the X and Y extents of the build area. Two linear artifacts, each 55 mm long, were arrayed by appending them end to end forming a single larger artifact of 110 mm in overall length. Four of these appended linear artifacts were positioned symmetrically about the center of the build area, beginning 8 mm from the build area origin, and ending 7 mm from the build area edges. These artifacts were termed as +XLA, -XLA, +YLA, and -YLA based on which coordinate axis they lie on. Additionally, a compound linear artifact (CLA), which is not defined in the standard, was placed in the +X/+Y quadrant of the build area oriented at 45° from the +X axis. The CLA was modeled as a scaled version of the standardized LA, such that its vertical faces were located at similar nominal X and Y positions as the corresponding faces on the +XLA and +YLA.

Two circular artifacts (CA) were included in the test piece. The first (CA1) was positioned close to the build area center with its center at (-21.21, 21.21) mm. The second (CA2) was positioned with its center at (94.19, 44.57) mm. The coarse, medium, and fine resolution holes (C-, M-, & F-RH), pins (C-, M-, & F-RP), and slots (C-, M-, & F-RS) were each placed within the build area as shown in Fig. 1. The fine configuration of each artifact was placed furthest in the recoat direction, in order minimize the effects of potential build failures. The

medium resolution ribs (M-RR) and surface texture artifacts (STA) were placed in the -X/-Y quadrant of the build area. All artifact abbreviations are summarized in Table 1.

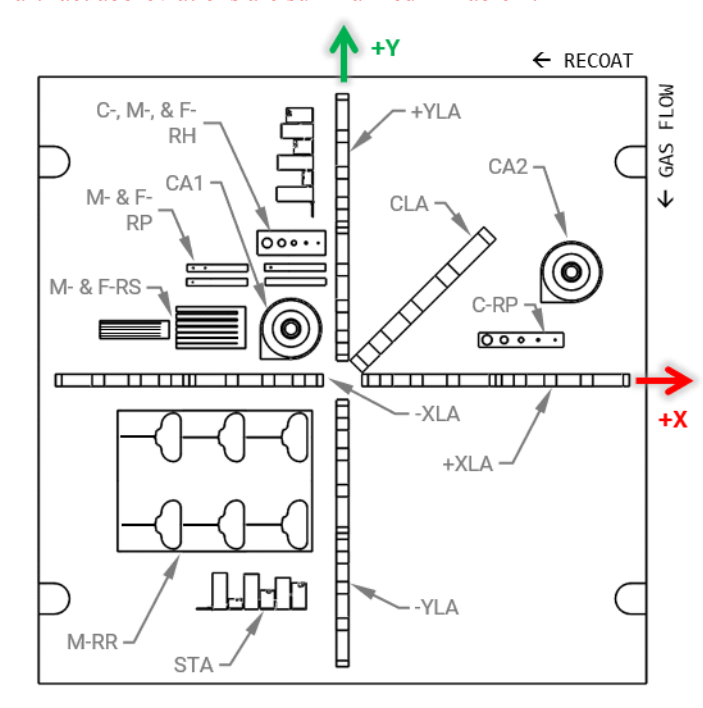


Fig. 1. Test piece design and artifact layout. A right-handed coordinate system is used. The +Z direction corresponds to the build direction.

Table 1. Table of artifact abbreviations

| Artifact(s) | Abbreviation(s) |
|---|------------------------|
| +X, -X, +Y, -Y linear artifacts | +XLA, -XLA, +YLA, -YLA |
| Compound linear artifact | CLA |
| Circular artifacts 1&2 | CA1, CA2 |
| Coarse, medium, & fine resolution holes | C-RH, M-RH, F-RH |
| Coarse, medium, & fine resolution pins | C-RP, M-RP, F-RP |
| Coarse, medium, & fine resolution slots | C-RS, M-RS, F-RS |
| Medium resolution ribs | M-RR |
| Surface texture artifact | STA |

3.2. Test piece manufacture

The designed artifact was manufactured on an EOS M280 LPBF system. The artifact was built on an annealed 1045 steel 252 x 252 mm build plate roughly 36 mm thick and surface ground. All artifacts were measured as-built and as-fused to the build plate. Virgin 316L powder supplied by EOS GmbH was used. Manufacturer provided material certifications report sieve analysis per ASTM B214 which shows 0.5% wt. content is captured by a 53 µm sieve and 0.0% wt. content is captured by a 63 µm sieve (sizes #270 and #230 per ASTM E11). Argon shielding gas was used during the build, and a standard tool steel straight-edge recoater blade was utilized. The artifact was built using manufacturer supplied process parameters, the most critical of which are specified in Table 2. Scan paths were planned using software native to the machine (EOS PSW). The 'stripes' scan strategy was used, which scans the infill region of a component slice using parallel stripes each made up of a raster scan pattern. Stripes change orientation by 27° between

layers. A contouring scan path, which is offset from the part outer surface by the user-set beam offset value, is also performed on each slice of each component after the infill region is scanned. Measurements of feature size and form primarily depend on the surfaces defined by these contouring scan paths. The build process spanned approximately 12 hours.

Table 2. LPBF process parameters.

| Parameter | Value |
|-------------------------|-----------|
| Layer height | 20 μm |
| Laser power | 195 W |
| Scan speed | 1083 mm/s |
| Hatch spacing | 90 μm |
| Beam diameter (approx.) | 80 μm |
| Build plate temperature | 80 °C |
| | |

Prior to manufacture of the test piece the AM machine was dimensionally assessed by the authors according to machine manufacturer recommended methods. A machine manufacturer defined test piece was built and measured with dial calipers per specified procedures. Measurements were used to calculate X and Y axis scaling corrections and beam offset. Calculation details are not provided by the manufacturer, only results are apparent to the machine users. The X and Y scaling corrections are expressed in units of percent while the beam offset is expressed in terms of millimeters. Prior to this user performed assessment, the machine manufacturer performed other system qualifications standard to machine commissioning, the details of which are not provided to the machine users.

3.3. Measurand definition and metrology methodology

Fig. 2 shows the +XLA, -XLA, +YLA, and -YLA, where each of the 18 vertical faces are labeled. The zeroth face is chosen in each case to be nearest to the build area origin. The only guidance provided in the standard for measurement of the LA is to acquire "positions of the cube faces relative to the primary datum at the end of the artifact." Notably, while this language suggests a vague form of measurement procedure, a rigorous definition in GD&T format is not provided. In this study, three major measurement procedures were executed on the LA. All three were evaluated using CMM data constituted of four probing points spread across each vertical cube face. The first measurement procedure determined the distance between the center points of planes fitted to the zeroth face and all other faces via a least-squares (LS) approach. The second measurement procedure, shown using ISO geometric product specifications (GPS) in Fig. 2, quantified the ability of the AM system to create accurate features of size by executing the same evaluation procedure, but only between the zeroth face and odd numbered faces, thus measuring the distance between opposing features. The zeroth face and each odd face were defined by LS fitting to the data, indicated by the circled "GG", which defines a global gaussian fit. The third measurement procedure, also shown using ISO GPS in Fig 2., evaluates the AM system's ability to position planes relative to a datum plane. This was evaluated according to the feature control frame noted in Fig. 2. The zeroth face serves at the datum feature that defines the datum reference frame (DRF) for all even numbered faces – the even faces are defined by an LS fit to the data, indicated by the circled "G", which defines a gaussian fit to the positioned feature. The -A- datum simulator was also constructed via LS.

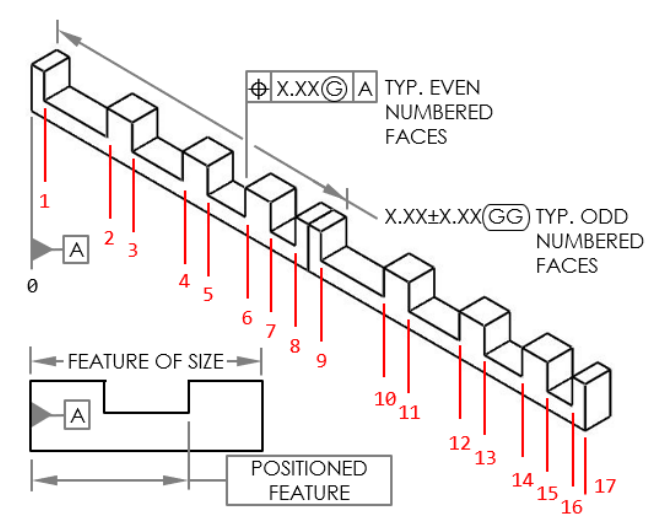


Fig. 2. Linear artifact measurand definitions.

The circular artifacts (CA) were evaluated for both size and form. Each CA is made of two rings, each ring with an outward facing boss-like feature and an inward facing bore-like feature. These four features are hereon termed the outer ring-outwards facing (O-O), outer ring-inwards facing (O-I), inner ringoutwards facing (I-O), and inner ring-inwards facing (I-I) cylindrical features. Each cylindrical feature was inspected using a CMM via three circular probing paths at heights of 2, 6, and 8 mm from the base of the cylinders. Size was evaluated as the diameter of a LS fit cylinder. Cylindricity was evaluated as defined in ISO 1101:2017 and ISO 12180-1:2011 as the peak-to-valley cylindricity deviation; the difference between the maximum and minimum points of deviation from the LS reference cylinder. The coarse resolution pins (C-RP) were evaluated for size and form in a similar manner. The 4 and 3 mm diameter pins were scanned with three evenly spaced circular paths and the 2 and 1 mm diameter pins with only two circular paths. The smallest C-RP was not inspected as this delicate feature did not survive the building process.

The resolution holes were evaluated for their size using gauge pins and a go/no-go methodology. Class ZZ minus pins available in 0.0127 mm increments were used. Holes 0.3 mm in nominal diameter and smaller were too small to be manually gauged with the available equipment and were not inspected. The resolution slots were also evaluated via go/no-go gauging using feeler gauges (no gauge class) available in 0.0254 mm increments. The resolution ribs were evaluated using a calibrated micrometer with a friction thimble, incremented in divisions of 0.00254 mm. Five local thickness measurements across the area of each rib were taken.

All CMM measurements were taken on a *Zeiss Micura*. The test piece was registered within the CMM coordinate system to establish a measurement coordinate system for CMM path planning. The machined surface of the build plate was used to as the primary alignment feature, defining the +Z axis orientation. The plane of symmetry between the zeroth faces of the positive and negative XLA defined the +X axis orientation.

The +Y axis orientation was defined as mutually orthogonal. The intersection of the plane fitted to the build plate surface and the planes of symmetry between the zeroth faces of the +/-XLA and +/-YLA defined the origin. The CMM utilized has a stated maximum permissible error of length measurement ($E_{0,MPE}$) of (0.8 + L/400) µm and was verified according to ISO 10360-2:2009. A coefficient of thermal expansion of 16.0 µm/m-K was used for temperature compensation. Relevant parameters of the measurement process for each artifact feature are provided in Table 3. Scanning speed was determined by the CMM software for optimal conditions. STA measurements are not presented in this study, as there is a wealth of prior work addressing surface texture of AM components. Readers are referred to reviews on the topic [4], [27].

Table 3. CMM measurement strategy parameters.

| Artifact feature(s) | Probe dia. [mm] | Method | Point spacing | No. of points |
|------------------------|--------------------|-----------------|---------------|---------------|
| LA vert. faces | 3.0 | Discrete points | N/A | 4 |
| CA1&2 O-O | 3.0 | Scanning | 0.021 | 3600 |
| CA1&2 O-I | 1.5 | Scanning | 0.014 | 3600 |
| CA1&2 I-O | 1.5 | Scanning | 0.007 | 3600 |
| CA1&2 I-I | 1.5 | Scanning | 0.0065 | 3600 |
| RP (4 mm) | 1.5 | Scanning | 0.0037 | 3600 |
| RP (3 mm) | 1.5 | Scanning | 0.0031 | 3215 |
| RP (2 mm) | 1.5 | Scanning | 0.0026 | 2535 |
| RP (1 mm) | 1.5 | Scanning | 0.002 | 1635 |

4. Results

4.1. Primary artifact measurements

Fig. 3 shows the plane-to-plane measurands for LA oriented on the system coordinate axes. Measurements are expressed as error from the nominal distance. The data does appear to be quite noisy, but some interesting aspects are evident. First, error from the nominal appears to be largest for faces that are further from the build area origin, with the exception of face 1 appearing to show some considerable error. Errors begin within a range of ± 0.035 mm but gradually grow with face number to be within a range of ± 0.085 mm.

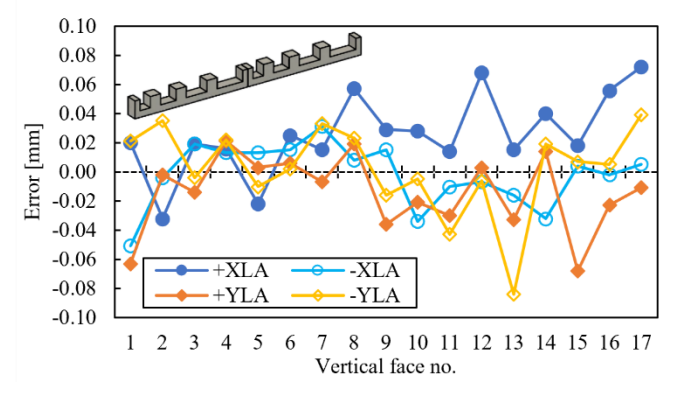


Fig. 3. Linear artifact error from the nominal plane-to-plane distance.

Fig. 4a and 4b characterize the LA via different measurands that translate well into a GD&T context. Fig. 4a shows

measurements of size between the zeroth face and all opposing faces in each LA (see Fig. 2). This measurand is influenced by effect of beam offset and beam positioning (i.e., scaling) error. An over-compensated beam offset results in opposing positive features that are both inwards of their nominal size while an under-compensated offset would result in the opposite. In contrast, the face position measurements presented in Fig. 4b are theoretically not influenced by beam offset. This is because the offset results in nominally the same translation of the datum face as well as the face positioned off the datum. For this measurand, it is expected that the effect of beam positioning errors will be more evident. Interestingly, for both measurands, the data appears somewhat less noisy when compared to the simple plane-to-plane measurements. This is possibly due to the fact that Fig. 3 presents measurements that alternate in terms of being influenced by beam offset error. The error values seen in Fig. 4a are negatively biased on the whole relative to the error values in Fig 4b. The negative shift of the respective curves between the two figures roughly represents the effect of removing beam positioning effects on these features of size. The mostly negative biases imply undersized features, which indicates an over-compensated beam offset. An examination of the CA can provide further insight.

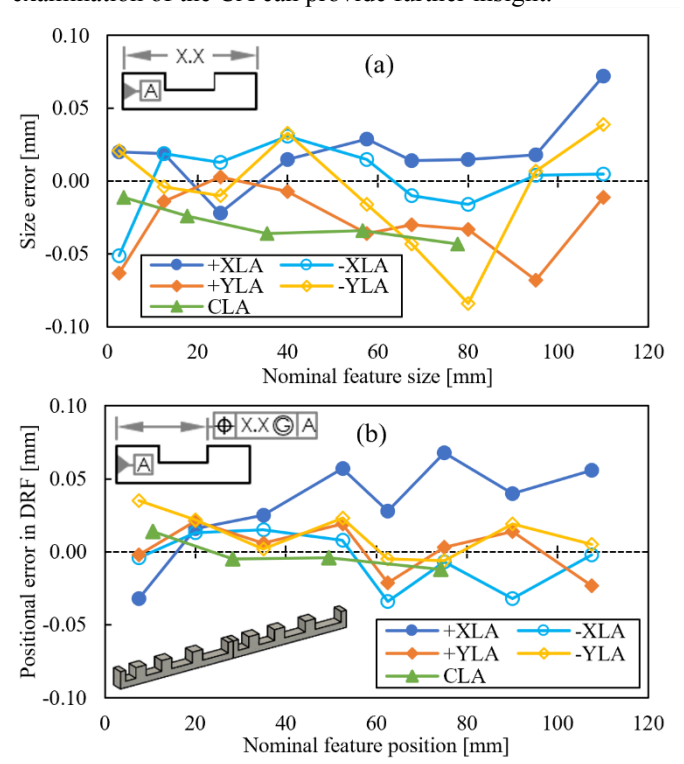


Fig. 4. (a) Linear artifact error from nominal feature size. (b) Linear artifact error from nominal feature position.

Error from the nominal diameters of CA1, CA2, and C-RP features are presented in Fig. 5a. All cylindrical features in this test piece, whether boss-like or bore-like, are consistently undersized. Errors range from -0.030 to -0.110 mm, trending larger with nominal feature diameter. This suggests beam positioning error that scales, but beam offset effects are not immediately apparent despite the LA suggesting their presence. Cylindricity measurements are shown in Fig. 5b. The C-RP that were measured exhibit a relatively steep increase in cylindricity with feature size while the CA shows somewhat consistent

cylindricity between the O-O, O-I, I-O, and I-I constituent features. The significant differences between the two smaller C-RP and the two larger may be due to only two circular probing paths being executed on these smaller features. More sampling is only likely to drive up form error. The form errors displayed are quite significant, ranging from roughly 0.070 to 0.130 mm for the larger C-RP and both CA. Form error does not detectably trend with feature size. Notably, CA1 and CA2 both exhibit similar cylindricity values for each constituent feature – features differ by 0.006 mm or less in cylindricity except for the O-O feature which differs by 0.022 mm. Taken in conjunction with the relatively similar diameter errors seen in Fig. 5, the AM system examined displays fair spatial repeatability of cylindrical features of this size scale.

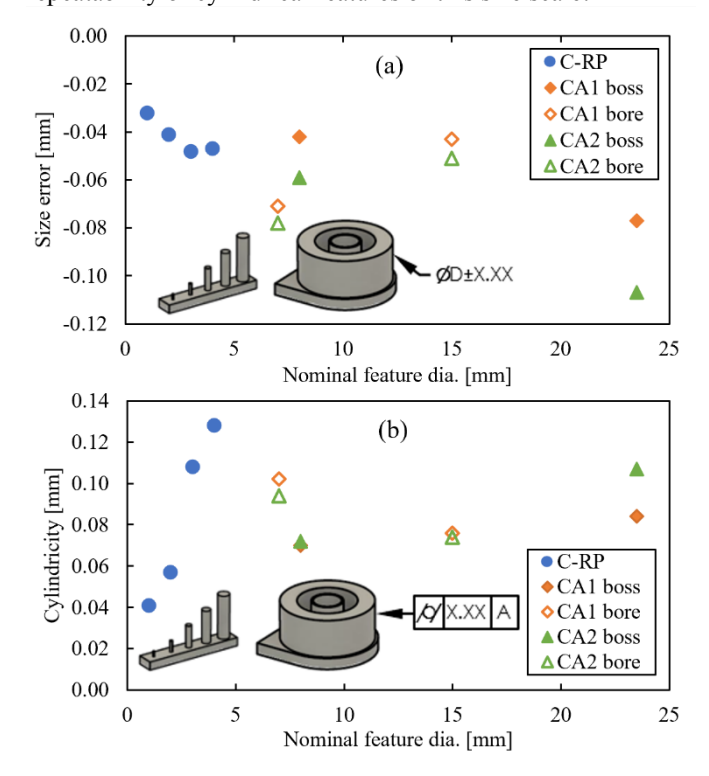


Fig. 5. (a) Cylindrical artifact and coarse resolution pin error from nominal feature diameter. (b) Cylindrical artifact and coarse resolution pin form error.

The go/no-go gauging results from the inspection of all resolution holes of sufficient size (greater than 0.3 mm nominal diameter) to be inspected with the available gauges are presented in Fig. 6. The nominal feature size is subtracted from the go and no-go gauge sizes to produce an error value range. It is worth noting that this form of measurement more closely approximates inscribing a feature of maximum size than it does fitting a feature via LS, resulting in a reported measurement that is smaller than what a LS procedure would report. All coarse resolution holes (4.0, 3.0, 2.0, 1.0, & 0.5 mm) and the three largest medium resolution holes (0.5 & 0.4 mm) successfully built. The results indicate size error of ± 0.025 mm or less for all holes 2 mm and larger. The holes under 1 mm that were measured are more severely undersized. At this small scale it is likely that partially fused powder particles on the hole cylinder surfaces have a more significant effect that reduced feature size. It should be noted that the 0.3 and 0.2 mm M-RH as well as the 0.2 mm F-RH can be visually observed. However, due to the lack of an appropriate measurement method, they cannot be definitively judged as building successfully or not.

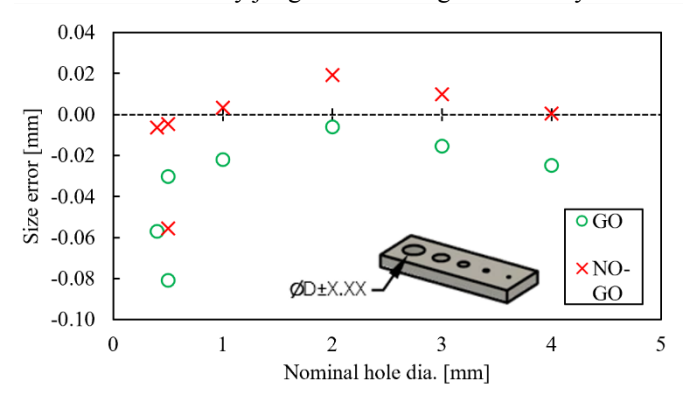


Fig. 6. Resolution hole error from nominal feature diameter.

The resolution slot go/no-gauging results are presented in a similar manner in Fig. 7. The five largest coarse resolution slots (1.0, 0.8, 0.6, 0.4, & 0.2 mm) built successfully. All slots 0.1 mm in nominal size and under did not accept any gauge size down to 0.0254 mm. Despite the visual presence of a slot down to even the smallest fine resolution slot (0.01 mm), these smaller slots were filled with enough trapped and partially fused powder particles that they did not accept any gauges. The slot width errors interestingly do not follow trends similar to the hole diameter errors. The go/no-go method identifies only the 0.6 mm slot as undersized, and the 0.8 mm slot as possibly undersized. The smallest slot is at least 0.143 mm oversized and seemingly the effect of partially fused powder particles earlier theorized does not apply in this case. It is of note is that these features exhibited some of the largest errors seen in any examined artifacts, with the 0.2 and 1.0 mm slots being at least 0.143 and 0.219 mm oversized. An explanation for this phenomenon is not immediately apparent.

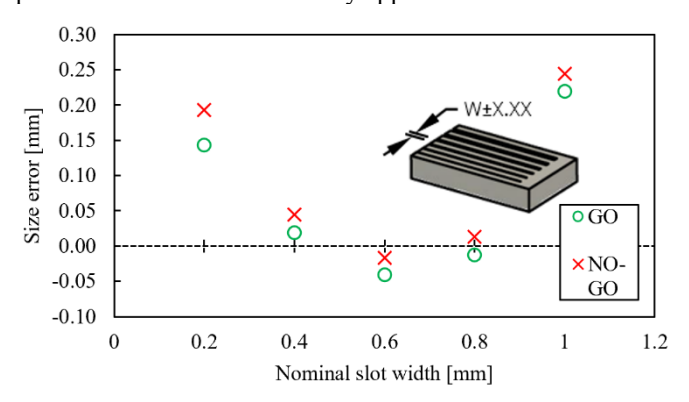


Fig. 7. Resolution slot error from nominal feature width.

The five largest medium resolution ribs successfully built, with the smallest (0.1 mm) having no evidence of any powder fused to create the feature. An examination of the build file shows that laser scan paths were planned for this feature – evidently the feature was too delicate to survive the build process. The means of five micrometer measurements of each rib are presented in Fig. 8 in terms of error from the nominal. Except for the 1.0 mm rib, the features are oversized in the range of 0.074-0.061 mm. Size error trends inversely with nominal rib width. The smaller ribs may build higher local temperatures during the AM process due to their small mass

and cross section, possibly leading to larger meltpools which increase feature width.

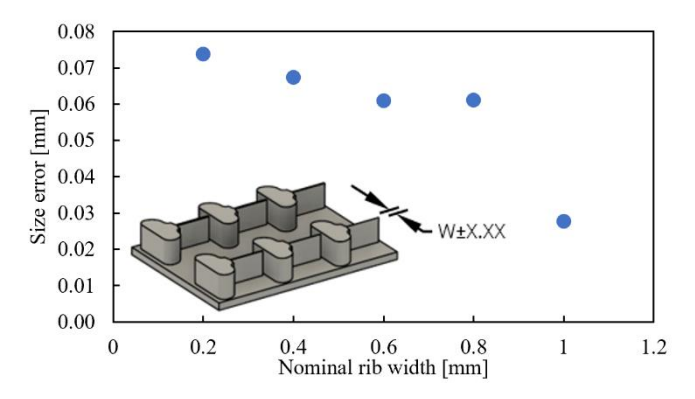


Fig. 8. Resolution rib error from nominal feature width.

4.2. Assessment of CMM measurement repeatability

Thus far, the measurements of a single CMM inspection routine have been reported. The measurement instrument is expected to produce repeatable measurements according to its specified capabilities on an ideal surface, however, AM surfaces are certainly not ideal. To address this concern a series of ten repeated measurements of the +XLA and CA1 were executed using the CMM strategies previously detailed. Table 4 shows the mean measurements of the CA1 features and their standard deviations. Fig. 9 shows the plane-to-plane measurements of the +XLA with error bars that represent ±(2*standard deviation), providing a representation of the scale of measurement repeatability compared to characteristic feature errors. In both cases, measurement standard deviation is slightly larger but on the order of error that would be predicted by $E_{0,MPE}$ at these length scales. In summary, the AM surfaces measured are non-ideal but not to a degree that produced repeatability issues on a scale that impacted the results presented in this work.

Table 4. Summary of CA1 O-O measurements.

| Measurand | Mean dia. [mm] | Std. dev. [mm] | Mean cyl. [mm] | Std. dev. [mm] |
|-----------|-------------------|-------------------|-------------------|-------------------|
| CA1 O-O | 23.422 | 0.0009 | 0.102 | 0.0139 |
| CA1 O-I | 14.959 | 0.0008 | 0.078 | 0.0018 |
| CA1 I-O | 7.955 | 0.0010 | 0.063 | 0.0034 |
| CA1 I-I | 6.932 | 0.0008 | 0.109 | 0.0020 |

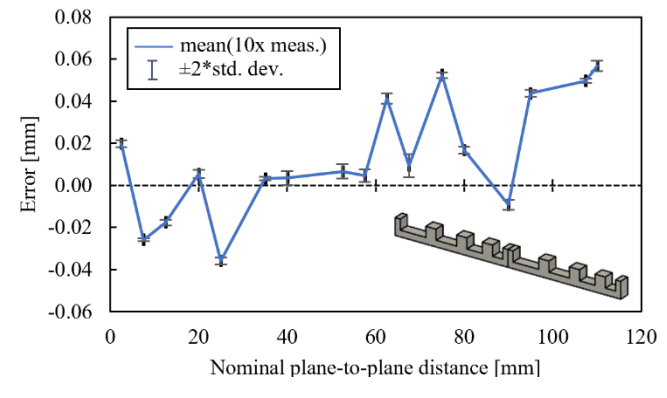


Fig. 9. Mean of 10x plane-to-plane distance measurements on the +XLA.

4.3. Stylus diameter effects

An important aspect of tactile probing that should not be overlooked when measuring rough surfaces is the effect of stylus size. The diameter of a spherical stylus acts a mechanical filter on rough surfaces, such as metal AM ones [20], [28]. In order to study this effect, the O-O feature of CA1 was inspected with three different stylus diameters, 5.0, 3.0, and 1.5 mm. Measurements with each stylus diameter were taken using the same measurement strategy as already described, only scanning speeds were reduced to half of normal operating conditions. Each measurement was repeated ten times. Diameter and cylindricity measurements were extracted as earlier described and are presented in Table 5. A one-way analysis of variance (ANOVA) was conducted in order to test for effects of stylus diameter. Results are presented in Table 6. The ANOVA reveals that stylus diameter affects the asmeasured feature diameter and cylindricity with a high degree of confidence (p < 0.001). The smaller stylus diameters result in smaller as-measured feature diameters and higher form error, with the smallest and largest stylus diameters producing a mean difference in diameter and cylindricity of 0.020 and 0.024 mm, respectively. These results follow conventional expectations, and implications are further analyzed in the discussion section.

Table 5. Summary of CA1 O-O measurements with varying stylus diameters.

| Measurand | Probe dia. [mm] | Mean dia. [mm] | Std. dev. [mm] |
|--------------|-----------------|----------------|----------------|
| Diameter | 1.5 | 23.406 | 0.0006 |
| Diameter | 3.0 | 23.419 | 0.0007 |
| Diameter | 5.0 | 23.426 | 0.0017 |
| Cylindricity | 1.5 | 0.104 | 0.0015 |
| Cylindricity | 3.0 | 0.088 | 0.0005 |
| Cylindricity | 5.0 | 0.080 | 0.0010 |

Table 6. One-way ANOVA on CA1 O-O diameter and cylindricity.

| Source | DoF | SS | MS | F | p |
|--------------|-----------------|----------|----------|---------|---------|
| | <u>Diameter</u> | | | | |
| Factor | 2 | 2.08E-03 | 1.04E-03 | 844.99 | < 0.001 |
| Error | 27 | 3.32E-05 | 1.23E-06 | | |
| Total | 29 | | | | |
| Cylindricity | | | | | |
| Factor | 2 | 3.17E-03 | 1.58E-03 | 1414.94 | <.0.001 |
| Error | 27 | 3.02E-05 | 1.12E-06 | | |
| Total | 29 | | | | |

A control experiment was conducted to show that these effects are due characteristics inherent to the AM components, not simply poor measurement methodology. A class ZZ gauge pin with a ground finish and diameter similar to the CA O-O feature was evaluated with the same CMM strategies. Measurements with a 1.5 and 5.0 mm probe repeated 10 times yielded diameter and cylindricity values, all differing by less than 1.0 μm . This effectively shows that the measurement variability due to stylus size may be isolated to characteristics of the AM surface.

4.4. Bias due to surface sampling

CMM data is constituted of a discrete set of points in coordinate space from which more complex measurements are derived. Whether using a discrete-point or scanning strategy the overall area of the component measured is relatively small which creates the possibility for bias in measurements derived from this data due to limited surface sampling. In this work, bias due to surface sampling is defined as a difference in derived measurements when only a portion of a feature surface is sampled in measurement as compared to when 100% of a feature surface is sampled, which serves as the reference measurement in this scenario. Simply put, different probing locations or scanning paths may capture distinct surface topography thereby producing unique data sets. In the case of low surface roughness components, such as those which are ground or machined, this effect is often considered negligible. In the case of an LPBF manufactured component, typical surface textures that exhibit high roughness as well as local peaks and valleys may cause this effect to be accentuated [20].

The +XLA and CA1 were inspected to study this effect. The +XLA was inspected via discrete-point probing according to the parameters already provided. The +XLA was also measured with a scanning strategy, also utilizing a stylus of 3.0 mm diameter that traces a rectangular path gathering data at 0.2 mm intervals. In each scenario three distinct probing routines were executed, where the second and third routines were offset in the +Z direction by 0.25 and 0.38 mm from the first points/path. Each routine was repeated five times to produce the mean error values presented in Fig. 10a and 10b, which show the results of discrete-point and scanning strategies, respectively. The scatter in measurements seen in both cases implies effects of bias due to surface sampling on each individual probing routine. Notably, scatter is reduced when a scanning strategy is used, as would be expected due to the larger surface sample.

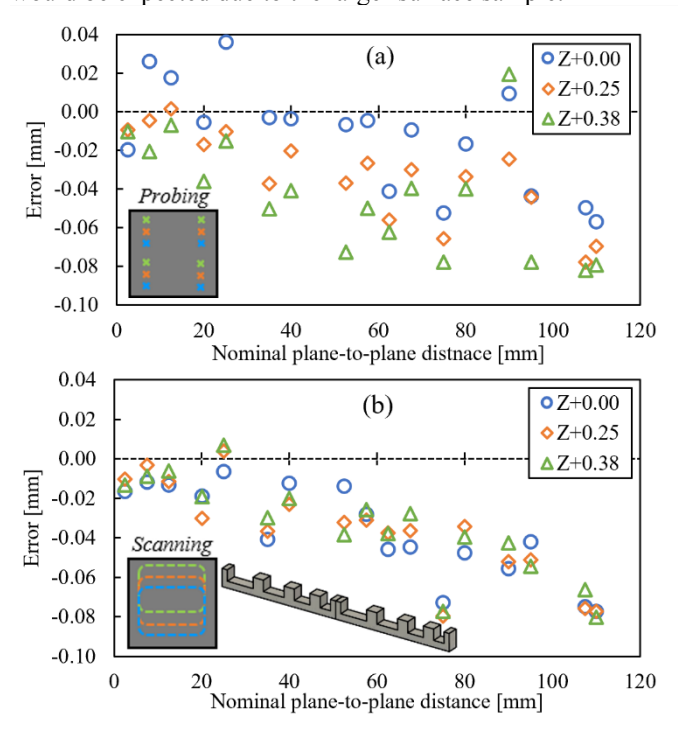


Fig. 10. Effect of surface sampling on the +XLA plane-to-plane distance using (a) discrete-points mode and (b) scanning mode.

To further study this phenomena CA1 was examined using the same strategies as earlier described. Three distinct scanning routines were each repeated five times. The second and third scanning paths were again offset in the +Z direction by 0.25 and 0.38 mm. The mean values of these measurements expressed in terms of error from the nominal are presented in Fig. 11. The magnitude of deviations between measurements derived from different surface samples of CA1 is slightly smaller than those for the +XLA, likely owing to the much larger surface sample of the CA1 features.

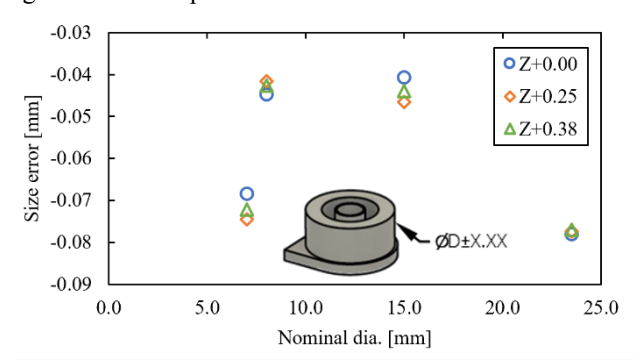


Fig. 11. Effect of surface sampling on CA1 O-O, O-I, I-O, I-O error from nominal feature diameter.

5. Discussion

5.1. AM system geometric performance diagnosis

As the standard suggests, the linear artifacts are the primary sources of information that might illuminate beam positioning error. Examining the results shown in Fig. 3 and 4a-b provides some insight into the performance of the beam steering galvanometers. The AM machine used has two galvos, each primarily responsible for maneuvering the beam in the X and Y axes. Fig. 4b shows very similar trends in positional deviation from the respective datum faces displayed by the positive and negative LA in each coordinate direction. In the case of the +YLA and -YLA not only are similar trends observed but error values are within 0.010 mm for the majority of measured faces. Note that these insights are possible as the effects of beam offset error have a minimal effect on the position of these features, thereby isolating beam positioning errors. Overall, these results indicate that galvanometer calibration profiles or mechanical behaviors are symmetric about the build area origin. Without further knowledge of galvanometer construction and controller architecture in-depth insight is limited. The size errors of the LA reported in Fig. 4a do not show the same trend, as the superposition of beam offset error on beam positioning error obfuscates insight into either error source. The plane-to-plane distances shown in Fig. 3 exhibit noisy behavior due to the alternating influence of beam offset error on every other data point. Evidently, the choice of linear artifact measurand significantly effects the discernibility of underlying AM machine geometric performance. While this information is not included in the standard, users would benefit from an understanding of which constituent error sources contribute to different measurands.

Referring to Fig. 10b provides even further insight. Here, the plane-to-plane distances of the +XLA acquired via a

scanning CMM measurement strategy over multiple surface samples are presented. The larger surface sample in each measurement results in higher repeatability, clarifying trends in the data. The plot exhibits a roughly linear trend of increasing error with distance from the build plate origin. Prior work form Lu et al. that directly evaluated beam positioning error, as opposed to artifact evaluation, on another EOS M280 presented a similar description of beam positioning error [29]. Error of a similar magnitude and trend is reported, but a far less noisy trend is present. Evidently, random process fluctuations in artifact manufacture and potential beam offset error have obfuscated this trend in the present work. These fluctuations in laser power, scan speed, local temperature, and powder bed quality play a significant role in determining the meltpool geometry, thus influencing the final component geometry. Of course, while a direct machine evaluation approach might provide strong insight into beam positioning errors, the artifact evaluation approach allows for an analysis that can enable tuning of an AM system to achieve desired geometric characteristics such as size and position in an end-component.

Examining Fig. 4a and Fig. 5a, which show the LA and CA size errors, should illuminate beam offset errors. Barring the influence of other factors, a consistent beam offset error should result in a consistent feature size error. These errors should be opposite in sign depending on whether the feature is positive, such as a boss, or negative, such as a bore (see Fig. 12a). That said, if significant beam positioning error effects are present, this prevents a simple application of this rule for all features of size throughout the build volume. As mentioned earlier, considering the bias between LA feature size errors (Fig. 4a) relative to feature position errors (Fig. 4b) is an approximation for removing beam positioning error effects. In this case the negative bias suggests an over-compensated beam offset. An important caveat to this diagnosis is that the small feature size and sparse surface sampling of the LA could have very well also contributed to exhibited biases – the relatively noisy trends in all LA measurements exemplify this.

An examination of the CA can provide further insight. All CA1 and CA2 cylindrical features are undersized and diameter errors matched closely between respective article features. The inwards facing features do not have a consistently more positive size error than the outwards facing features - this implies that beam offset error effects are overwhelmed by other phenomena. The C-RP diameters shown in Fig. 5a also are all undersized, and the smaller pins appear to be less undersized than the larger pins. This may have been partly due to temperature building during the AM process in these small cross-sectional area components, thereby leading to larger meltpools which increased feature diameter. Taken together, CA1, CA2, and C-RP errors all indicate gross beam positioning scale error, as larger features generally have more negative size error. The +XLA measurements in Fig. 10b support this claim, as they show that the AM system is undershooting its commanded beam position. Additionally, the CA2 features (located further from the origin) are slightly more undersized than the CA1 features, which follows with the +X scaling error suggested by Fig. 4b.

Consider the simplified cases presented in Fig. 12. Several simplifying assumptions are made – X and Y beam-positioning

error is assumed to scale linearly with distance from the build area origin and the CA is considered to be centered on the origin. Fig. 12a displays the expected changes should an overor under-compensated beam offset be present – both rings either shrink or grow due to a uniform translation of all feature surfaces. Fig. 12b shows the results of over-scaled or underscaled X and Y beam positioning, resulting in all surfaces moving out or in with error magnitude scaling with feature size. Fig. 12c provides an example of the superimposed effects of an over-compensated beam offset and under-scaled beam positioning error – a condition that appears to be present in the examined AM machine. Plotting these diameter errors would result in the plot shown in Fig. 12d, assuming no effects of random process fluctuations. Comparing to Fig. 5a confirms that the beam positioning system is undershooting its commanded value, but either a minimal beam offset error is present (thus the pattern in Fig. 12d is not shown) or other confounding effects dominate. The latter seems most likely, due a lack of consistency in how the boss-like and bore-like features are related to each other in Fig 5a.

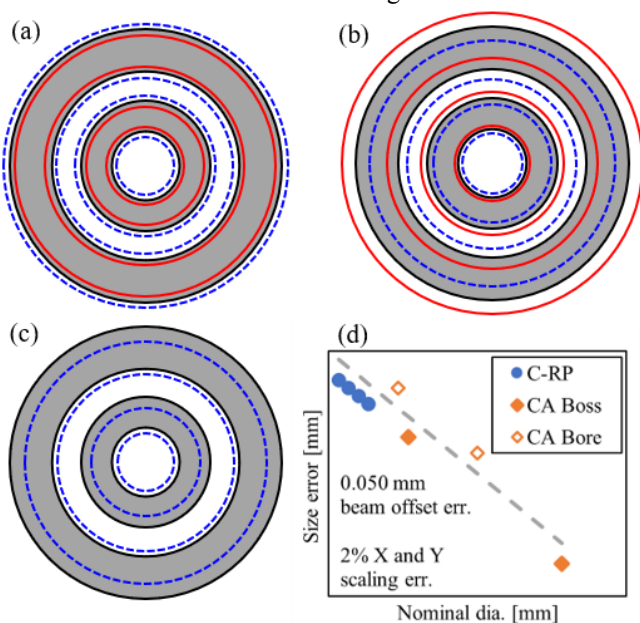


Fig. 12. Theorized effects on the CA in the case of: (a) Over- (solid red) and under-compensated (dashed blue) beam offset (b) Over- (solid red) and under-scaled (dashed blue) X & Y beam positioning. (c) Superimposed effects of an over-compensated beam offset and under-scaled X & Y beam positioning. (d) Size error for case c. The dashed line represents the trend for size error if there was zero beam offset compensation error.

Those applying this standard should use caution if they look to the smallest positive resolution-type features to study beam offset error. In this case local temperature rise during the AM process may significantly affect meltpool geometry. Negative features, such as the RH and RS, should also be disregarded when assessing beam offset error. They are difficult to measure with CMMs and mechanical gauging. Optical methods will bias measurements as opposed to LS fitting of CMM data. Further, trapped powder and partially fused particles will similarly bias measurements.

In all of these measurements it is difficult to distinguish the effect that beam distortion may have. The F-theta lens used in this AM system to focus the laser on to a planar field may

produce distortion of the beam energy distribution profile that varies over the build area. General knowledge of these optical systems suggests the most extreme distortion occurs at the lens edges. Additionally, the beam incidence angle to the build plane varies from orthogonal over the build area. This causes the beam spot shape to elongate, resulting in a lower heat intensity. The interaction of these phenomena and their effects on meltpool geometry is complex. Decoupling the effects from what appears to be beam positioning or offset error also proves a challenge. Further study of this complex problem is required. It should be noted that no acquired measurements attempt to address in the build platform positioning system. While several articles could be inspected in a manner to provide this insight none were in order to limit the scope of this study. Readers are referred to Lu et. al, who performed in in-depth direct evaluation of Z positioning, straightness, and orientation [29].

Decoupling of error sources in AM machines is plainly a major challenge despite the several methods presented in this work. Further studies that intentionally alter certain AM machine parameters (e.g. beam offset, X/Y scaling) with larger samples sizes would help address these current implementation challenges by exemplifying typical effects on artifact measurands. Further, it is important to establish the limits of AM machine error that artifact measurements can detect – once machine errors have been sufficiently minimized random process fluctuations out of the user's control may dominate. Establishing this limit may be an important step to defining allowable error values in commercial AM system performance.

5.2. Measurement strategy for AM components

CMMs are likely to be favored when implementing this standard due to their automation capabilities, relatively high accuracy and repeatability, and built-in software for realizing complex measurement procedures. Unfortunately, this approach can result in sparse sampling of feature surfaces. However, methods that cover greater surface area, such as Xray computed tomography and optical methods like structured light scanning are not perfect alternatives, as these techniques have limitations due to their large or complex uncertainty budgets and issues measuring large and deep features [30], [31]. Acknowledging that CMMs will be used to implement this standard requires that the effects of bias due to surface sampling be accounted for. As has been demonstrated, different CMM probing points or scanning paths can significantly affect discrete-point strategies with different surface samples resulting in measurement differences as great as 0.050-0.070 mm in some cases. Scanning strategies should be favored when at all possible, and high surface coverage should be strived for.

An inspector's choice of stylus diameter should be carefully considered, and manufacturing engineers should consider specifying stylus diameter for every feature of interest when developing test piece inspection protocols. This is essential if these artifacts are to be used for control monitoring of AM machines over time and use. Choosing a large stylus diameter might be favored should the aim be to evaluate features as they would function in an assembly – the large diameter will more closely simulate how surfaces interact at scale. However, smaller diameters probes will reduce the mechanical filtering

effect of tactile measurement and lead to LS feature fits that better represent the true surface. Notably, the LS approach is less prone to being influenced by random process fluctuations and partially fused powder particles that produce local peaks, and thus will provide better insight into base AM machine performance issues. This should be strongly considered by inspectors that consider other fitting algorithms. It should be noted that new provisions in several ISO standards allow for mathematical fittings to be rigorously defined in a standard drawing context, and users may consider whether these tools can be leveraged for their specific needs [32].

While artifacts such as the LA, CA, and possibly the coarse configurations of the resolution artifacts are likely to be evaluated with CMMs, most resolution-type artifacts present exceedingly small features that will likely require alternate metrology tools. The standard does recommend the use of calibrated optical microscopes, but this method will only accurately evaluate a very small portion of these deep features. Consider the M-RR, M-RH, and F-RH which each had features that showed visual evidence of being present but would not accept gauges far below their nominal sizes. Despite modern metrology tending towards automation and digitization it would seem this is a case for manual gauging.

5.3. Commentary on ISO/ASTM 52902

The configurability of the artifacts provided for in the standard appears to be a strength. For the EOS M280 system used in this study every type of artifact was easily adapted and positioned to produce a test piece with a wide variety of artifacts that span the build area. The resolution type artifacts were all available in size ranges that assessed the limitations of the AM system studied at a reasonable level of granularity. Arraying the LA allowed for them to be used as intended.

As has been noted, rigorous definitions of artifact measurands are not provided and it has been demonstrated that the choice of the measurand can reveal different qualities of the AM system at hand. In particular, the exact measurands extracted from the LA directly affect which aspects of error in the AM machine can be effectively diagnosed. Similarly, without a rigorous definition it would be easy for different inspectors to derive unique measurements on the same artifact. This is not to say that the standard must provide a single and unambiguous measurand definition, though this would address the issue. As is consistent with flexible nature of the standard it seems the best response is for users to establish procedures which guide repeatable practices that suit their needs.

Further examples of this issue manifest in the fitting algorithms used with both the LA and CA. Both artifacts lend themselves towards CMM measurement and this means users have important choices to make when fitting features to acquired measurement data. LS methods are easily implemented with CMM data, and ISO product definition standards tend to favor feature definition via these algorithms [33]–[35]. That said, LS fitting results in measurements that may deviate from the functional behavior of a feature. For example, when creating a boss that must fit into a bore minimum circumscribed or maximum inscribed feature fitting methodologies will better describe the feature. ASME product

definition standards tend to favor definition of true geometric counterparts in this manner [36], [37]. That said, these methods are prone to being thrown off by highly local surface topography variations – also likely with AM components. Further, if careful attention is not paid to making consistent choices, comparisons of test piece measurements may be extremely misleading.

The as-designed artifact dimensions appear to present some issues as well. The clearance between several artifact features requires uncommonly small stylus diameters and careful path planning. Most importantly, the small vertical faces of the LA do not allow for large surface samplings. LA measurands are critical to evaluating beam positioning and offset error, and in this study the effects of both random process fluctuations and bias due to surface sampling have resulted in unrepeatable measurements and noisy trends. The size and aspect ratio of several other artifacts also present practical inspection issues. The larger resolution holes could be measured with CMMs, but their shallowness requires exceptionally small stylus sizes and prevents the effective evaluation of cylindricity. This also makes mechanical gauging difficult, as the only the very tip of a gauge pin fits and the inspector perceptions of go or no-go are difficult to delineate. Resolution type artifacts that some users might wish to inspect via optical methods are short enough that they can be difficult to separate from the build plate in order to bring to a microscope bench. The surface roughness artifacts also present practical difficulties as they are designed. Their size and lack of integrated support geometry make them difficult to extract while avoiding damage to the surfaces.

6. Conclusions

A number of geometric artifacts constituting a single test piece were manufactured on a LPBF system and measured per the practices described by ISO/ASTM 52902. The AM machine was calibrated per manufacturer specification prior to artifact manufacture, simulating implementation of this standard to monitor system performance in a commercial environment. A CMM was used to evaluate the LA, CA, and C-RP, while manual gauging techniques were used to inspect all other resolution type features. Critical implementation practices, auxiliary to those provided in the standard, have been identified. Particularly, specific measurands, metrology techniques, and modes of analysis that detected AM machine errors were highlighted for future users of the standard. The conclusions from this study are summarized below.

- AM machine geometric parameters were assessed. Beam positioning errors that appeared to scale with distance from the build area origin were uncovered. An over-compensated beam offset error was suspected, though its presence may have been masked by the beam positioning errors.
- Linear artifact measurements implied a degree of symmetry
 to beam positioning error about the build area origin.
 Complex, non-linear calibration profiles may be required to
 tune beam positioning and thereby produce feature positions
 with minimal error. Further user knowledge and control of
 commercial AM systems would be required.
- The effects of beam offset and X/Y beam positioning error are difficult to decouple in the case of several artifact

- measurands. Certain measurands of the LA that isolated individual error sources were identified. The effects of both AM machine error types on the CA were discussed, and methods for decoupling the error sources were implemented and extended in theory.
- Random AM process fluctuations were significant contributors to the error displayed in many artifact measurements of a well-qualified AM machine.
- Rigorous measurand definition is absolutely required in implementation of this standard. Measurands that appeared similar at the surface level were revealed to highlight different AM machine errors when closely studied.
- Measurement strategy for AM surfaces must be carefully considered when implementing this standard. CMM scanning strategies with excellent feature surface coverage reduced the effect of random process fluctuations on measurands. Stylus diameter must be well defined and consistently implemented according to the user's goals. LS feature fitting procedures appeared favorable for several purposes of machine diagnosis. Manual gauging appeared to be favored when assessing resolution type artifacts.

Acknowledgements

This work was supported in part by the Department of Energy [DE-EE0008303] and the National Science Foundation [CMMI-1646013, CMMI-1825640 and IIP-1631803].

References

- M. Kamal and G. Rizza, "Design for metal additive manufacturing for aerospace applications," in *Additive Manufacturing for the Aerospace Industry*, Elsevier, 2019, pp. 67–86.
- [2] M. Seifi, A. Salem, J. Beuth, O. Harrysson, and J. J. Lewandowski, "Overview of Materials Qualification Needs for Metal Additive Manufacturing," *JOM*, vol. 68, no. 3, pp. 747–764, Mar. 2016, doi: 10.1007/s11837-015-1810-0.
- [3] S. Moylan, J. Slotwinski, A. Cooke, K. Jurrens, and M. A. Donmez, "An Additive Manufacturing Test Artifact," *J. Res. Natl. Inst. Stand. Technol.*, vol. 119, p. 429, Oct. 2014, doi: 10.6028/jres.119.017.
- [4] R. K. Leach, D. Bourell, S. Carmignato, A. Donmez, N. Senin, and W. Dewulf, "Geometrical metrology for metal additive manufacturing," *CIRP Ann.*, pp. 1–24, Jun. 2019, doi: 10.1016/j.cirp.2019.05.004.
- [5] ASTM International, "ISO/ASTM 52902-19 Additive manufacturing — Test artifacts — Geometric capability assessment of additive manufacturing systems," ASTM International, West Conshohocken, PA, 2019.
- [6] International Organization for Standardization, "ISO 230 series: Test code for machine tools," Geneva, Switzerland.
- International Organization for Standardization, "ISO 10791 series:
 Test conditions for machining centres," Geneva, Switzerland.
- [8] ISO, "ISO IS 10791-7: 1998, Test conditions for machining centers--Part 7: Accuracy of a finished test piece.," Geneva, Switzerland, 1998.
- [9] NAS, "NAS, 979 Uniform Cutting Tests--NAS series metal cutting equipment specifications," 1969.
- [10] The American Society of Mechanical Engineers, "ASME B5.54, Methods for Performance Evaluation of Computer Numerically Controlled Machining Centers," New York, NY, 2005.
- [11] S. Moylan, A. Cooke, K. Jurrens, J. Slotwinski, and M. A. Donmez, "A Review of Test Artifacts for Additive Manufacturing," National Institute of Standards and Technology, NIST IR 7858, May 2012. doi: 10.6028/NIST.IR.7858.
- [12] M.-A. de Pastre, S.-C. Toguem Tagne, and N. Anwer, "Test artefacts for additive manufacturing: A design methodology review," *CIRP J. Manuf. Sci. Technol.*, vol. 31, pp. 14–24, Nov. 2020, doi: 10.1016/j.cirpj.2020.09.008.

- [13] B. S. Rupal, M. Secanell, and A. J. Qureshi, "Geometric Benchmark Test Artifact for Laser Powder Bed Fusion Process.," presented at the 2nd Conference of NSERC Network for Holistic Innovation in Additive Manufacturing (HI-AM), Vancouver, BC, Canada, 2019.
- [14] J. P. Kruth, "Material Incress Manufacturing by Rapid Prototyping Techniques," CIRP Ann., vol. 40, no. 2, pp. 603–614, 1991, doi: 10.1016/S0007-8506(07)61136-6.
- [15] M. Mahesh, "Rapid prototyping and manufacturing benchmarking," National University of Singapore, 2004.
- [16] Mahesh M., Wong Y.S., Fuh J.Y.H., and Loh H.T., "Benchmarking for comparative evaluation of RP systems and processes," *Rapid Prototyp. J.*, vol. 10, no. 2, pp. 123–135, Jan. 2004, doi: 10.1108/13552540410526999.
- [17] L. Rebaioli and I. Fassi, "A review on benchmark artifacts for evaluating the geometrical performance of additive manufacturing processes," *Int. J. Adv. Manuf. Technol.*, vol. 93, no. 5–8, pp. 2571– 2598, Nov. 2017, doi: 10.1007/s00170-017-0570-0.
- [18] P. Jacobs and J. Richter, "Accuracy," in *Rapid Prototyping & Manufacturing: fundamentals of stereolithography*, Society of Manufacturing Engineers, 1992, pp. 287–315.
- [19] B. S. Rupal, R. Ahmad, and A. J. Qureshi, "Feature-Based Methodology for Design of Geometric Benchmark Test Artifacts for Additive Manufacturing Processes," *Procedia CIRP*, vol. 70, pp. 84– 89, 2018, doi: 10.1016/j.procir.2018.02.012.
- [20] V. M. Rivas Santos, A. Thompson, D. Sims-Waterhouse, I. Maskery, P. Woolliams, and R. Leach, "Design and characterisation of an additive manufacturing benchmarking artefact following a design-formetrology approach," *Addit. Manuf.*, vol. 32, p. 100964, Mar. 2020, doi: 10.1016/j.addma.2019.100964.
- [21] B. Kruth, J. Van Vaerenbergh, and P. Mercelis, "Benchmarking of different SLS/SLM processes as rapid manufacturing techniques," presented at the Int. Conf. Polymers & Moulds Innovations (PMI), Gent, Belgium, 2005.
- [22] H.-S. Byun and K. H. Lee, "Design of a New Test Part for Benchmarking the Accuracy and Surface Finish of Rapid Prototyping Processes," in *Computational Science and Its Applications — ICCSA* 2003, Berlin, Heidelberg, 2003, pp. 731–740.
- [23] W. F. Mitchel, D. C. Lang, T. A. Merdes, E. W. Reutzel, and G. S. Welsh, "Dimensional Accuracy of Titanium Direct Metal Laser Sintered Parts," p. 14.
- [24] V. Brøtan, "A new method for determining and improving the accuracy of a powder bed additive manufacturing machine," *Int. J. Adv. Manuf. Technol.*, vol. 74, no. 9–12, pp. 1187–1195, Oct. 2014, doi: 10.1007/s00170-014-6012-3.
- [25] Y. Tang et al., "Accuracy Analysis and Improvement for Direct Laser Sintering," 2004.
- [26] S. Moylan, J. Slotwinski, A. Cooke, K. Jurrens, and M. A. Donmez,

- "Proposal for a standardized test artifact for additive manufacturing machines and processes," presented at the Solid Freeform Fabrication Symposium, Austin, TX, 2012.
- [27] A. Townsend, N. Senin, L. Blunt, R. K. Leach, and J. S. Taylor, "Surface texture metrology for metal additive manufacturing: a review," *Precis. Eng.*, vol. 46, pp. 34–47, Oct. 2016, doi: 10.1016/j.precisioneng.2016.06.001.
- [28] S. Lou, X. Jiang, W. Sun, W. Zeng, L. Pagani, and P. J. Scott, "Characterisation methods for powder bed fusion processed surface topography," *Precis. Eng.*, vol. 57, pp. 1–15, May 2019, doi: 10.1016/j.precisioneng.2018.09.007.
- [29] Y. Lu, "Experimental sampling of the Z-axis error and laser positioning error of an EOSINT M280 DMLS machine," *Addit. Manuf.*, p. 16, 2018.
- [30] A. du Plessis and E. Macdonald, "Hot isostatic pressing in metal additive manufacturing: X-ray tomography reveals details of pore closure," *Addit. Manuf.*, vol. 34, p. 101191, Aug. 2020, doi: 10.1016/j.addma.2020.101191.
- [31] P. I. Stavroulakis and R. K. Leach, "Invited Review Article: Review of post-process optical form metrology for industrial-grade metal additive manufactured parts," *Rev. Sci. Instrum.*, vol. 87, no. 4, p. 041101, Apr. 2016, doi: 10.1063/1.4944983.
- [32] E. P. Morse, C. M. Shakarji, and V. Srinivasan, "A Brief Analysis of Recent ISO Tolerancing Standards and Their Potential Impact on Digitization of Manufacturing," *Procedia CIRP*, vol. 75, pp. 11–18, 2018, doi: 10.1016/j.procir.2018.04.080.
- [33] International Organization for Standardization, "ISO 1101:2017 Geometrical product specifications (GPS) — Geometrical tolerancing — Tolerances of form, orientation, location and run-out," Geneva, Switzerland, 2017.
- [34] International Organization for Standardization, "ISO 17450-1:2011 Geometrical product specifications (GPS) — General concepts — Part 1: Model for geometrical specification and verification," Geneva, Switzerland, 2011.
- [35] International Organization for Standardization, "ISO 14405-1:2016 Geometrical product specifications (GPS) — Dimensional tolerancing — Part 1: Linear sizes," Geneva, Switzerland, 2016.
- [36] The American Society of Mechanical Engineers, "ASME Y14.5 -2018, Dimensioning and Tolerancing," New York, NY, 2018.
- [37] The American Society of Mechanical Engineers, "ASME Y14.5.1 -2019, Mathematical Definition of Dimensioning and Tolerancing Principles," New York, NY, 2019.